JACS
JOURNAL OF THE AMERICAN CHEMICAL SOCIETY
Article
pubs.acs.org/JACS

A Mechanistic Rationale for the 9-Amino(9-deoxy)*epi* Cinchona Alkaloids Catalyzed Asymmetric Reactions via Iminium Ion Activation of Enones

Antonio Moran,[†] Alex Hamilton,[†] Carles Bo,[†,‡] and Paolo Melchiorre*[,†,§]

[†]Institute of Chemical Research of Catalonia, ICIQ, Avenida Països Catalans 16, 43007 Tarragona, Spain
[‡]Department de Química Física i Inorgànica, Universitat Rovira i Virgili (URV), Marcel.li Domingo, 43007 Tarragona, Spain
[§]Institució Catalana de Recerca i Estudis Avançats (ICREA), Passeig Lluís Companys 23, 08010 Barcelona, Spain

Supporting Information

ABSTRACT: The 9-amino(9-deoxy)*epi* cinchona alkaloids have expanded the synthetic potential of asymmetric aminocatalysis, enabling the highly stereoselective functionalization of a variety of sterically hindered carbonyl compounds. However, there is a lack of basic understanding of the mechanisms of cinchona-based primary aminocatalysis. Herein, we describe how a combination of experimental and theoretical mechanistic studies has revealed the origin of the stereoselectivity of the Friedel−Crafts alkylation of indoles with α,β-unsaturated ketones catalyzed by 9-amino(9-deoxy)*epi* quinine. An essential role for the achiral acid cocatalyst is uncovered: upon condensation of the cinchona catalyst with the enone, the resulting covalent imine intermediate and the acid interact to build-up a well-structured ion-pair supramolecular catalytic assembly, which is stabilized by multiple attractive noncovalent interactions. All the components of the assembly cooperatively participate in the stereocontrolling event, with the anion of the achiral acid being the structural element responsible for the π-facial discrimination of the iminium ion intermediate.

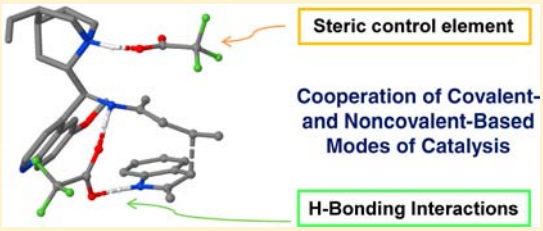

INTRODUCTION

Asymmetric aminocatalysis[1] exploits the potential of chiral primary and secondary amines to catalyze the asymmetric functionalization of unmodified carbonyl compounds. The strategy is based on fundamental mechanistic patterns, using the chemistry of simple enamine and iminium ion intermediates. Chiral cyclic secondary amines, in particular proline[2a] and its derivatives, including diarylprolinol ethers[2b] and phenylalanine-derived imidazolidinones,[2c] have shown broad versatility and efficiency, providing a reliable synthetic platform for the asymmetric functionalization of linear aldehydes and enals at their α, β, γ,[3] and even ε[4] positions (Figure 1).[5] Recently, the "tools of the trade" of traditional physical organic chemistry have been used to gain a detailed mechanistic understanding of the complex multistep processes inherent to secondary amine catalysis, revealing the elements responsible for stereocontrol.[6]

The 9-amino(9-deoxy)*epi* cinchona alkaloids **1a−f** (Chart 1) are primary amines easily derived from natural sources.[7] They have recently been recognized as a general catalyst class for expanding the applicability and synthetic potential of aminocatalysis.[8] The cinchona-based primary amines have enabled the stereoselective functionalization of a variety of sterically hindered carbonyl compounds, which cannot be functionalized using secondary amines and which are often elusive substrates for metal-based approaches too. Remarkably, this single catalyst class can activate carbonyl compounds characterized by completely distinct structural features and steric bias (e.g., simple ketones as well as α-branched substituted aldehydes and ketones, and their α,β-unsaturated counterparts),[9] while exploiting the different aminocatalytic activation modes (Figure 1).[10] The consistently high level of stereocontrol inferred testifies to their versatility and reliability.

The lack of basic understanding of the mechanisms inherent to cinchona-based primary aminocatalysis[11] stands in sharp contrast to the extensive experimental studies that have delineated its reactivity. To date, the mechanistic speculations mainly come from empirical deductions, which are useful for extrapolating qualitative mechanistic models. It is, however, clear that the synthetic potential of the 9-amino(9-deoxy)*epi* cinchona alkaloids can be fully exploited only by an intimate appreciation of the catalytic mechanism and by identifying the elements essential for stereocontrol.

We recently began a program aimed at combining[12] experimental studies and kinetic analysis with computational methods[13] in order to obtain fundamental insights into the mechanism of cinchona-based primary amine catalysis. The asymmetric Friedel−Crafts-type alkylation of indoles **2** with α,β-unsaturated ketones **3** was selected as the model reaction (Scheme 1). This process marked the appearance in the chemical literature of amines **1** as effective catalysts for

Received: April 8, 2013
Published: June 7, 2013

dx.doi.org/10.1021/ja404784t | J. Am. Chem. Soc. 2013, 135, 9091−9098

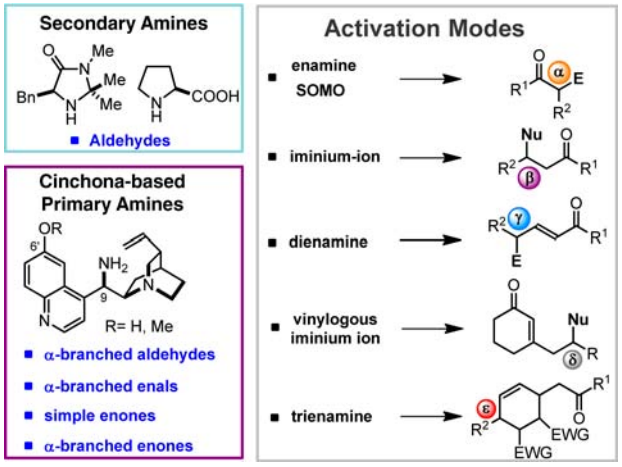

Figure 1. The state-of-the-art of asymmetric aminocatalysis: six distinct activation modes enable the direct stereoselective functionalization of unmodified carbonyl compounds. While secondary amines provide an efficient way of functionalizing unsubstituted aldehydes, the cinchona-based primary amines offer the possibility of effecting processes with sterically demanding partners. E: electrophile; Nu: nucleophile; EWG: electron-withdrawing group.

Chart 1. Cinchona-Based Primary Amine Catalysts

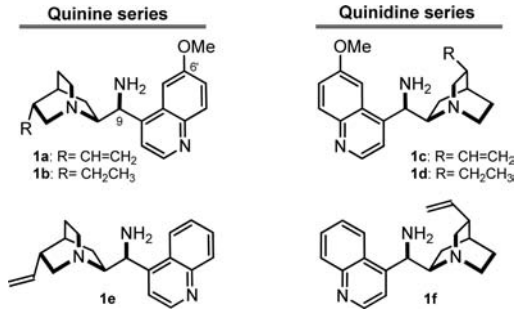

Scheme 1. Asymmetric Friedel–Crafts Alkylation of Indoles via Iminium Ion Activation of Simple Enones

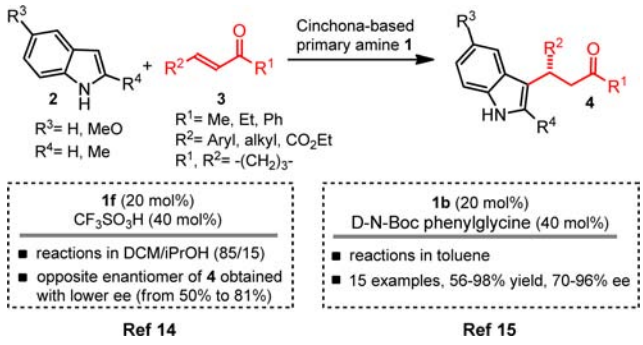

asymmetrically functionalizing carbonyl compounds. At the start of 2007, Chen's group[14] and us,[15] independently, applied this catalyst class to the iminium ion activation of α,β-unsaturated ketones. Chen and colleagues used the cinchonine-based catalyst (**1f** in Chart 1) in combination with 2 equiv of a strong acid, such as trifluoromethanesulfonic acid, to catalyze the stereoselective addition of indoles to enones in good yield yet moderate enantiomeric excesses.[14] At the same time, we were studying the same transformation using the hydroquinine-derived catalyst **1b**.[15] In agreement with Chen's study, we observed a moderate level of enantioselectivity (ee in the range of the 70s) when using a strong acid cocatalyst (i.e., trifluoroacetic acid, TFA). The key element to engineering a highly selective catalyst was the use of a weak acid.[16] Indeed, the catalytic amine salt made by combining **1b** and D-*N*-Boc phenylglycine, promoted the Friedel–Crafts alkylation, inferring a higher level of stereocontrol (ee of adducts **4** in the range of the 90s, Scheme 1).

These initial investigations soon highlighted a distinct feature of catalysis by cinchona-based primary amines **1**: the possibility of modulating both the reactivity and the stereoselectivity of the iminium ion-catalyzed transformation by tuning the nature of the acid cocatalyst. These observations were translated into empirical models that were later used in many other applications.[9,10] However, a rational understanding of the precise role played by the acid was not advanced.

Herein, we describe how a combination of experimental and theoretical studies, by means of density functional theory (DFT), has revealed the origin of the stereoselectivity of the Friedel–Crafts alkylation of indoles via iminium ion activation of α,β-unsaturated ketones catalyzed by 9-amino(9-deoxy)*epi*-quinine (**1a**). The study uncovers an essential role for the achiral acid cocatalyst: first it assists the cinchona catalyst condensation with the enone. Then, the acid interacts with the resulting covalent imine intermediate to build-up a well-structured ion-pair supramolecular catalytic assembly, which is stabilized by multiple attractive noncovalent interactions.[17] All the components of the assembly cooperatively participate in the stereocontrolling event, with the anion of the achiral acid being the structural element responsible for the π-facial discrimination of the iminium ion intermediate. This study further establishes the key role of the counteranion in asymmetric transformations proceeding via iminium ion activation[18] and may lay the foundations for future developments in the area of cinchona-based primary aminocatalysis.

RESULTS AND DISCUSSION

Experimental Mechanistic Studies. The Friedel–Crafts alkylation of 2-methylindole (**2a**) and (*E*)-3-octen-2-one (**3a**) promoted by the 9-amino(9-deoxy)*epi*-quinine **1a** in toluene was selected as the prototypical reaction for mechanistic analysis (Scheme 2). In accordance with the original reports,[14,15] we confirmed that an acid cocatalyst is needed to power the catalytic functions of amine **1a**;[19] otherwise, the catalyst remains inactive.

The initial investigations also confirmed how the nature of the acid cocatalyst, in particular the p*K*a,[16] greatly influences the reaction rate as well as the level of stereoselectivity. Scheme

Scheme 2. Effect of different acid co-catalysts on the model reaction

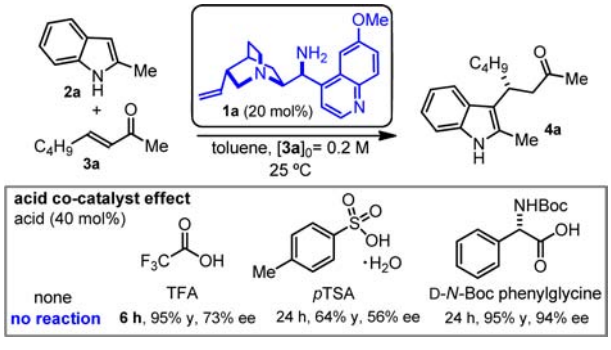

dx.doi.org/10.1021/ja404784t | J. Am. Chem. Soc. 2013, 135, 9091–9098

2 reports the results obtained with three distinct acids (*p*-toluenesulfonic acid monohydrate (*p*TSA), *N*-Boc-D-phenylglycine, and TFA). Given the high reactivity induced by TFA (the model reaction reached completion over 6 h at ambient temperature and over 2 h at 45 °C) and the fact that the cinchona primary amine-TFA combination has found wide application in highly stereoselective iminium ion transformations of enones,[9a,d,20] this catalytic system was subjected to deep mechanistic analyses.

Effect of the Acid Concentration. We first evaluated the effect of the TFA concentration on the model reaction. The reaction of **2a** (0.24 M) and enone **3a** (0.20 M) catalyzed by amine **1a** (0.04 M) in toluene at 45 °C was repeated over a range of concentrations of TFA (from 0.024 to 0.119 M). These experiments were conducted in the presence of hexamethylphosphoric triamide (HMPA, 1.75 ratio with respect to [TFA])[21] needed to suppress a nonstereoselective acid-promoted background reaction[22] catalyzed by TFA (extensive details are provided in Section B within the Supporting Information, SI).[23] As depicted in Figure 2, while

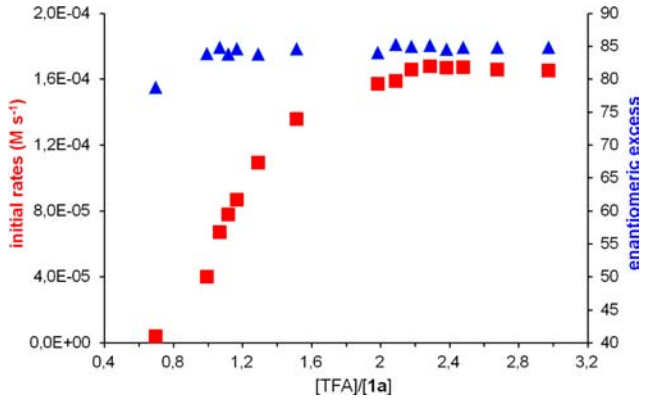

Figure 2. Plot of the initial reaction rates (■, red) and of the enantioselectivity (▲, blue) for the model reaction at different [TFA]/[**1a**] ratios. Conditions: 45 °C, [**2a**] = 0.237 M; [**3a**] = 0.198 M; [**1a**] = 0.04 M; [TFA] = 0.024−0.119 M; [HMPA] = 0.042−0.217 M, adjusted to keep [HMPA]/[TFA] = 1.75;[21,23] freshly distilled HMPA was dried over 4 Å molecular sieves to exclude the presence of water. The initial rates were obtained by linear regression of the product concentration [**4a**] vs time data obtained before 10% conversion (using HPLC sampling, see Figures S5 and S8 within SI for details).

the enantioselectivity of the reaction is rather insensitive to the amount of TFA,[21] the reaction rate remains relatively slow when <1 equiv of TFA with respect to **1a** is present. A strong acceleration is observed once the concentration of the acid becomes higher than [**1a**], reaching a maximum at a 2.3:1 ratio of TFA to **1a**. This indicates that a second equivalent of TFA is needed to achieve an effective catalytic system. The 2.3:1 ratio of TFA to the cinchona catalyst **1a** was selected for further mechanistic studies.

Kinetic Studies. The reactivity of our model reaction (conversion in the range of the 90 s over 2 h at 45 °C) makes it suitable for reaction progress kinetic analysis (RPKA),[24] a useful approach to identify the rate-determining step in complex catalytic reactions. The progress of the reaction of **2a** and **3a**, catalyzed by the **1a**·$(TFA)_{2.3}$ combination[25] in the presence of HMPA (1.75 ratio with respect to TFA) at 45 °C, was in situ monitored in a reaction calorimeter (Figure 3).[26] Full details of our RPKA are given in Section D of the SI.

The global catalytic reaction kinetic was studied by applying the "excess" ([*e*] = [**2a**] − [**3a**], excess of one substrate over another) experiment method and the graphical rate equation methodology developed by Blackmond.[24] "Same excess" experiments were carried out to establish whether consistent kinetic behavior was maintained throughout the course of the entire reaction. The overlap of kinetic runs executed at different initial concentrations but the same excess of [**2a**] relative to enone [**3a**] ([*e*] = 0.1 M) and plotted as reaction rate vs [**3a**] (runs **a** and **b** in Figure 3a) reveals that no significant catalyst deactivation occurs. In two further experiments, the absolute catalyst concentration was varied ([**1a**] = 0.03−0.04 M, from 15% to 20 mol %) while maintaining the same initial substrate concentrations. There was perfect overlay when plotting the reaction rate normalized to the catalyst concentration (i.e., the turnover frequency of the catalyst) versus the limiting reagent [**3a**]. This indicated a first-order dependence on the catalyst (Figure 3b). Three more experiments using "different excess" conditions gave information about the reaction order on the indole and the enone. The overlay observed when normalizing the reaction rate to [**2a**] versus [**3a**] reveals that the reaction is first order in the indole **2a** concentration (Figure 3c). However, the slight curvature observed in the graphical rate equation plot suggests a complex order in [enone].[24b] This was further corroborated by the plot reported in Figure 3d, showing that the rate/[**3a**] vs [**2a**] plots do not overlay.

We have conducted further kinetic experiments, by reaction calorimetric monitory, in the presence of different amounts of water (15 and 30 mol %). These studies, labeled as runs **a**′ and **a**″, are detailed in Figure 3a. They show how the presence of water slightly inhibited the reaction.

From nonlinear regression analysis of the kinetic data, the empirical rate equation (written in the "power-law" form, eq 1]) was determined.[25,27]

$$\text{rate}(\text{M min}^{-1}) = k\cdot[\mathbf{1a}\cdot(\text{TFA})_{2.3}]^{1.0}\cdot[\mathbf{2a}]^{0.98}\cdot[\mathbf{3a}]^{0.77}$$
$$k = 3.6 \pm 0.3\text{M}^{15/4}\text{min}^{-1} \quad (1)$$

The information acquired allowed a critical interrogation of the generally accepted mechanism for the iminium ion-based conjugate addition to enones catalyzed by **1a**, as depicted in Scheme 3. The reversible condensation of the cinchona-based primary amine **1a** with enone **3a**, aided by TFA, determines the formation of the iminium ion intermediate **A**. The resulting electronic effect renders the *β*-carbon atom of the unsaturated system more susceptible to nucleophilic attack by lowering the energy of the lowest unoccupied molecular orbital (LUMO). The LUMO-lowering effect drives the conjugate addition of indole **2a**. The carbon−carbon bond-forming event results in the intermediate **B**, which, after hydrolysis, gives the final adduct **4a** and regenerates the catalyst **1a**. The RPKA indicates that the rate of the model reaction depends on the concentration of both the nucleophile **2a** and the enone **3a**. This implies that the rate-determining step is neither the iminium ion formation (to give species **A**) nor the final hydrolysis step involving intermediate **B**.

The inhibition effect of water, as detailed in Figure 3a, further confirms that the release of the product **4a**, while regenerating the catalyst is not rate limiting. Thus, the indole addition to the iminium ion **A** represents the rate- and the stereoselectivity-determining step of the reaction.[28]

The slight curvature observed in the graphical rate equation plots of Figure 3c, normalized to [**2a**], also suggests that the

dx.doi.org/10.1021/ja404784t | *J. Am. Chem. Soc.* 2013, 135, 9091−9098

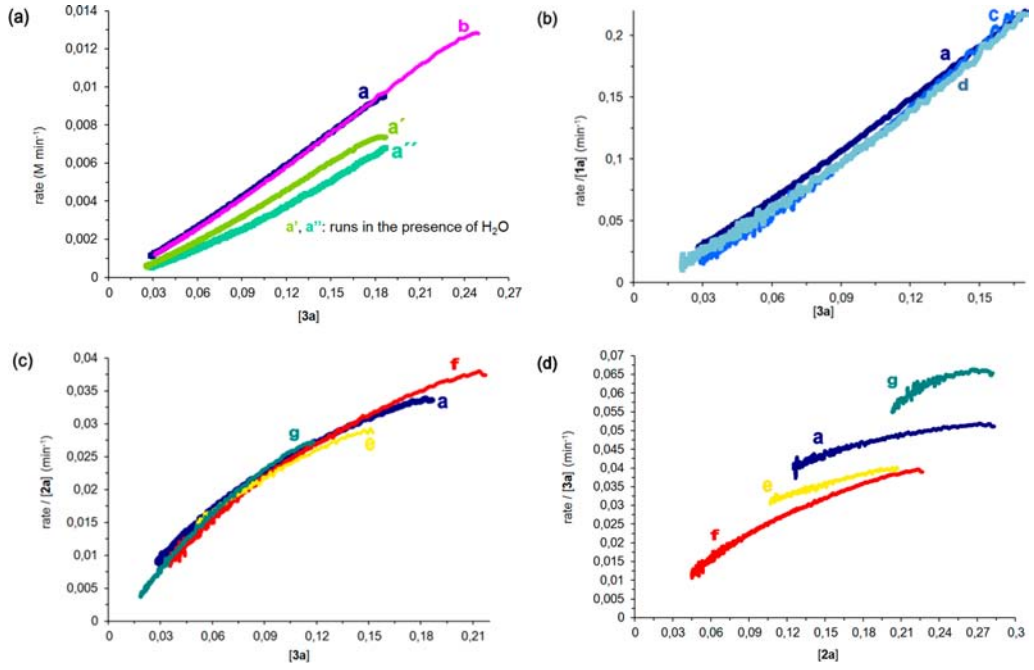

Figure 3. Reaction progress kinetic profiles measured by calorimetry for the model reaction under the standard conditions:[25] toluene, 45 °C, using **1a**·$(TFA)_{2.3}$ as the catalyst and with [HMPA] adjusted to keep [HMPA]/[TFA] = 1.75.[21,23] Freshly distilled HMPA was dried over 4 Å molecular sieves before use. Note that reaction progress is from right to left. For consistency, all kinetic analyses used data from 10 to 90% conversion of enone [**3a**]. (a) "Same excess" experiments, [*e*] = 0.1 M: checking for catalyst stability and for the effect of water on the reactivity. (b) Kinetic experiments at different catalyst concentrations (15−20 mol %): probing the reaction order in [**1a**·$(TFA)_{2.3}$]. (c) and (d) "Different excess" experiments, [*e*] = 0.1, 0.06, 0.01, and 0.17 M: exploring dependence on substrates [**2a**] and [**3a**] concentrations. Reaction conditions: (**a**): [**1a**] = 0.040 M, [TFA] = 0.093 M, [HMPA] = 0.164 M, [**2a**] = 0.304 M, [**3a**] = 0.207 M; (**a′**) [**1a**] = 0.040 M, [TFA] = 0.093 M, [HMPA] = 0.161 M, [**2a**] = 0.305 M, [**3a**] = 0.199 M, [H_2O] = 0.027 M; (**a″**) [**1a**] = 0.040 M, [TFA] = 0.092 M, [HMPA] = 0.161 M, [**2a**] = 0.304 M, [**3a**] = 0.204 M, [H_2O] = 0.061 M; (**b**) [**1a**] = 0.040 M, [TFA] = 0.093 M, [HMPA] = 0.163 M, [**2a**] = 0.367 M, [**3a**] = 0.274 M; (**c**) [**1a**] = 0.035 M, [TFA] = 0.080 M, [HMPA] = 0.144 M, [**2a**] = 0.299 M, [**3a**] = 0.206 M; (**d**) [**1a**] = 0.030 M, [TFA] = 0.069 M, [HMPA] = 0.122 M, [**2a**] = 0.299 M, [**3a**] = 0.207 M; (**e**) [**1a**] = 0.040 M, [TFA] = 0.092 M, [HMPA] = 0.163 M, [**2a**] = 0.225 M, [**3a**] = 0.169 M; (**f**) [**1a**] = 0.040 M, [TFA] = 0.092 M, [HMPA] = 0.162 M, [**2a**] = 0.249 M, [**3a**] = 0.240 M; (**g**) [**1a**] = 0.040 M, [TFA] = 0.092 M, [HMPA] = 0.162 M, [**2a**] = 0.301 M, [**3a**] = 0.136 M.

Scheme 3. Simplified Catalytic Cycle for the Model Friedel−Craft Alkylation Catalyzed by 1a·$(TFA)_2$ (ref 25)[a]

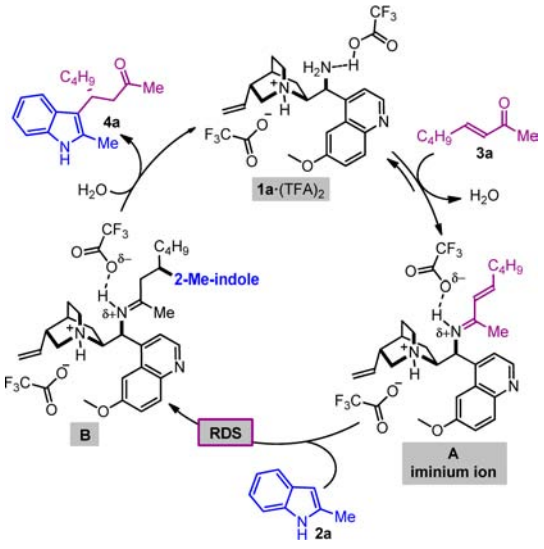

[a]The crucial role of TFA in assisting the iminium ion formation is carefully detailed in Scheme 4.

equilibrium is not fully driven toward the iminium ion intermediate **A**, resulting in a complex noninteger order in the enone **3a** concentration. This scenario is consistent with a catalytic cycle under steady-state conditions with the catalyst partitioned between the free state **1a**·$(TFA)_2$ and the intermediate **A**. Thus, a definitive resting state cannot be identified, with the catalyst concentration shared between different intermediates.

From the empirical rate equation in eq 1, we performed an Eyring analysis, measuring the rate constants at seven different temperatures between 30 and 60 °C. The obtained data were fitted using the Eyring equation (Figure 4), which revealed an activation enthalpy ($\Delta H^{\ddagger}$) of +9.2 ± 0.2 kcal·mol^{-1} and an activation entropy ($\Delta S^{\ddagger}$) of −35.6 ± 0.7 cal·mol^{-1}K^{-1}. The large negative value of the entropic contribution suggests an associative process prior to the rate-limiting step and a high degree of order required in the transition state. This provides an additional argument for C−C bond formation as the rate-determining step.

Computational Studies. We used DFT to elucidate the origin of the stereoselectivity.

Methods. The geometries for all the intermediates and transition-state structures were optimized in vacuo by using the metahybrid DFT functional M06-2X[29a] together with 6-31G(d) basis set. The equilibrium structures were verified to have all real positive harmonic vibrational frequencies and the transition structures to have only one imaginary frequency. Zero-point vibrational energy, enthalpic, and entropic corrections have been obtained from unscaled frequencies at 318 K with M06-2X/6-31G(d). The solvation free energies in toluene were computed consistently at the same level, using the universal

dx.doi.org/10.1021/ja404784t | J. Am. Chem. Soc. 2013, 135, 9091−9098

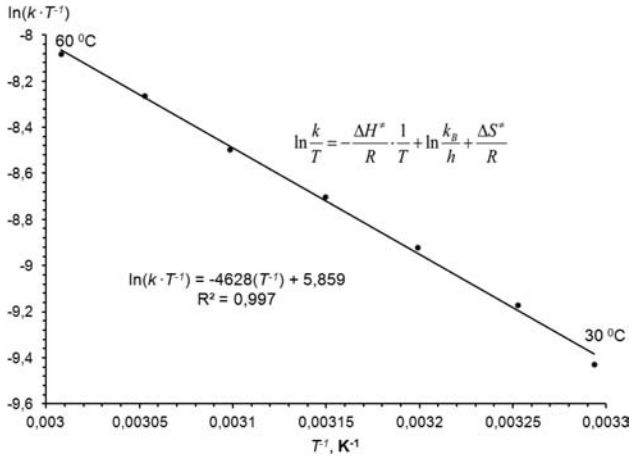

Figure 4. Eyring plot for the model Friedel–Craft alkylation catalyzed by 20 mol % of **1a**·$(TFA)_{2.3}$ and in the presence of HMPA (1.75 ratio with respect to TFA). R = 1.9859 cal/mol·K, k_B (Boltzmann constant) = 3.30×10^{-24} cal/K, and h = 1.58×10^{-34} cal·s.

solvation model SMD.[29b] Because of the relevance of the C–C bond forming step, the energies of the related transition-state structures were refined with single-point calculations including solvent effects at the M06-2X/6-311++G(d,p) level. Gibbs free energies in solution, including all computed corrections, are reported in the text. All computations were performed using Gaussian 09.[29c]

We first explored the condensation of amine **1a** with the enone substrate, leading to the iminium ion formation. Of particular interest throughout the mechanism was the crucial importance of 2 equiv of the acid (TFA) required for activation.[19] We focused on a model system formed by amine **1a**, two associated TFA molecules,[25] and (*E*)-pent-3-en-2-one (**3b**) as a simplified electrophile (Scheme 4). The starting point was taken as the isolated molecules, and all energies are given as relative free energy, ΔG_{318}.

The molecular assembly **5** (amine **1a**, **3b**, and the two TFA molecules) is stabilized by an intricate network of hydrogen bonds, which somewhat overcome the large entropic contribution to the free energy (ΔG_{318} = 2.7 kcal mol^{-1}). One TFA molecule is engaged in electrostatic interaction with the more basic site of **1a**, resulting in the protonation of the tertiary amino moiety, while the second TFA molecule is bridging both the primary amine and the carbonyl group of enone **3b** by means of hydrogen bonds. The last selective hydrogen-bond interaction activates the enone substrate, facilitating the amine nucleophilic attack and a simultaneous proton transfer to the carbonyl oxygen (**TS5**), with a barrier of 9.5 kcal·mol^{-1}. The resulting aminol intermediate (**6**) is stabilized by a hydrogen-bonding network, where one TFA molecule bridges between the (cationic) primary amino moiety and the hydroxyl group of the aminol, while the other TFA molecule acts as a counteranion to the protonated tertiary amine, concurrently hydrogen bonding to the primary amino group. The position of the TFA associated with the tertiary amine is critical to the next step of the mechanism, which is the proton transfer from the primary ammonium nitrogen atom to the hydroxyl group of the aminol **7**. The calculations identified an acid assisted mechanism, which uses the oxygen of the tertiary amine-associated TFA anion as the 'pivot point' to transfer the proton, as the favored pathway for the proton transfer (barrier of 5.6 kcal·mol^{-1}). This further highlights the need for both equivalents of the acid, in agreement with the experimental observations.

From the intermediate (**7**), the mechanism proceeds via partial dissociation of the water molecule with a barrier of 7.4 kcal·mol^{-1} (**TS7**) to give the intermediate (**8**), which is approximately 10.2 kcal·mol^{-1} more stable than **7**. Although the H_2O molecule in **8** is stabilized by hydrogen bonds, its

Scheme 4. Reaction Free Energy (ΔG_{318}) Including Solvent Effects for the Formation of the Iminium Ion (A)[a]

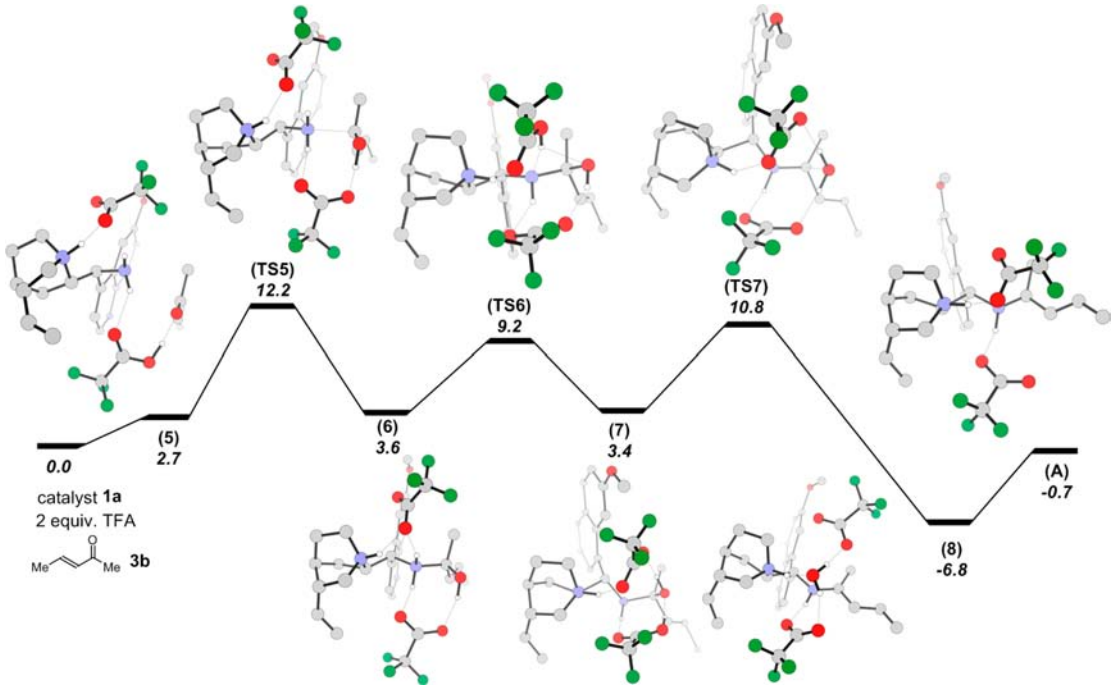

[a]Values in kcal·mol^{-1}; M06-2X/6-31G(d)/SMD//M06-2X/6-31G(d).

dx.doi.org/10.1021/ja404784t | J. Am. Chem. Soc. 2013, 135, 9091–9098

complete dissociation to give the iminium ion assembly **A**[30] requires only 6.1 kcal·mol^{-1} in the reaction free energy profile.

We then focused on the C−C bond forming step (Scheme 5).[31] The association of **2a** with the intermediate **A** leading to

Scheme 5. Reaction Free Energy (ΔG_{318}) Including Solvent Effects for the Rate- and Stereoselectivity-Determining Step[a]

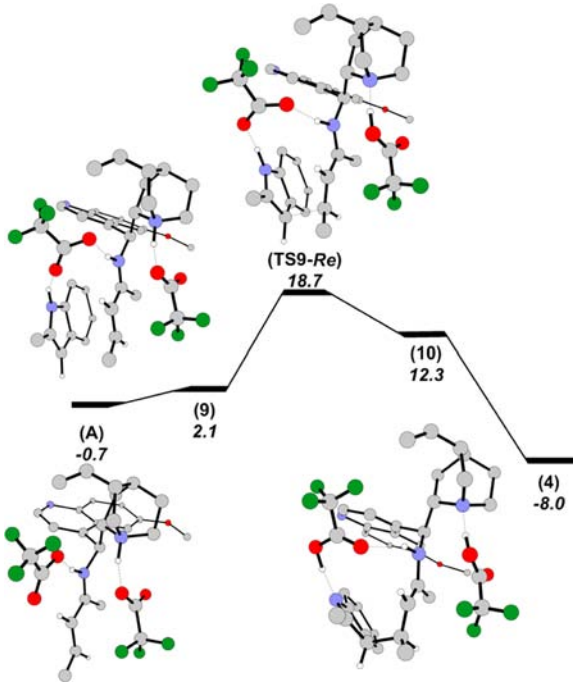

[a]Values in kcal·mol^{-1}; M06-2X/6-31G(d)/SMD//M06-2X/6-31G(d).

the molecular assembly **9** is uphill due to entropic contributions. Again, the acid molecules play an important role in stabilizing the overall structure, with the N−H moiety of the incoming indole **2a** being engaged in hydrogen-bonding interactions with the trifluoroacetate anion associated with the iminium ion. This peculiar 'directing' interaction is experimentally supported by the low reactivity and enantioselectivity observed when using an N-methyl protected indole.[15] From **9**, the carbon−carbon bond formation has a barrier of 16.6 kcal·mol^{-1} (**TS9**), and therefore an overall barrier of 18.7 kcal·mol^{-1}. The product of the carbon−carbon bond formation (**10**) is approximately 10.2 kcal·mol^{-1} less stable than **9** and rapidly loses a proton to restore aromaticity and to form the final Friedel−Crafts product **4**, with regeneration of the catalyst **1a**·$(TFA)_2$. Computed energies indicate that the C−C bond forming step (**TS9-*Re***) in Scheme 5) has a free energy barrier 6.5 kcal·mol^{-1} higher than the iminium ion formation (**TS5** in Scheme 4), thus identifying the nucleophilic attack of 2-methylindole **2a** to the iminium ion **A** as the rate-determining step, in agreement with the kinetic studies.

The computed most stable transition-state assembly **TS9-*Re*** (Figure 5a) shows that the achiral acid cocatalyst is the stereochemical-defining element responsible for the π-facial discrimination of the iminium ion intermediate. Indeed, the trifluoroacetate anion, which is engaged in the electrostatic interaction with the protonated tertiary amino moiety of the chiral cinchona catalyst, effectively shields the *Si*-face of the reactive π-system. This induces the approach of the nucleophile from the less congested *Re*-face. This process leads to the

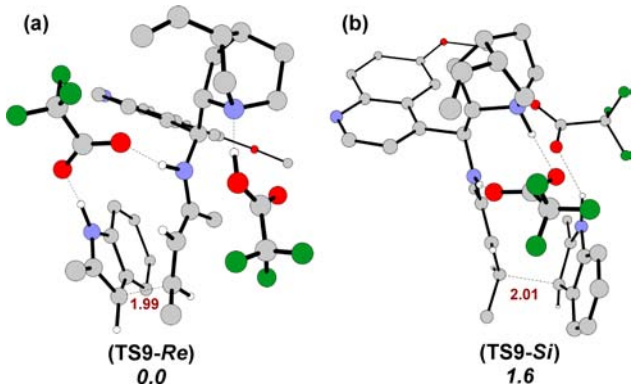

Figure 5. Optimized transition-state structures for the (a) *Re* and (b) *Si* face addition of indole **2a** to the iminium ion assembly **A**. Selected bond distances are in Å. Relative free energies (DDG_{318}) given in kcal·mol^{-1}; M06-2X/6-311++G(d,p)/SMD//M06-2X/6-31G(d).

formation of the experimentally observed *R* enantiomer of the product **4**. The formation of the opposite enantiomeric product would result from the indole addition to the *Si* face of the iminium ion intermediate (**TS9-*Si*** in Figure 5b), with an energetic penalty of 1.6 kcal·mol^{-1} paid for structurally repositioning the anion. This relates to a calculated enantiomeric excess of ~85%, in good agreement with the experimental value (the addition of **2a** to (*E*)-pent-3-en-2-one **3b** at 45 °C gives the corresponding product in 70% ee). The theoretically predicted values of the activation parameters for the rate-limiting transition state **TS9** ($\Delta H^{\ddagger}$ = +8.9 kcal·mol^{-1} and $\Delta S^{\ddagger}$ = −22.1 cal·mol^{-1}K^{-1} at 318 K), taking as reference the intermediate **5**, are in reasonable agreement with the values experimentally determined with the Eyring analysis (Figure 4).

As already mentioned, the trifluoroacetate anion associated with the iminium ion has a directing effect (through attractive noncovalent interactions) on the incoming indole. This hydrogen-bonding motif aligns the indole in the correct orientation prior to C−C bond formation as well as stabilizes the transition state. For the preferred *Re* face addition pathway the C−C distances in the intermediate **9** and TS are 3.14 and 1.99 Å respectively, whereas for the *Si* face approach the distances are 3.75 and 2.01 Å. The orientation for *Re* face addition manifold leads to a better overlap of the frontier orbitals (HOMO/LUMO) in the intermediate prior to C−C bond formation, as shown in Figure 6. This preferential orientation further contributes to the lower barrier for the *Re* face approach transition state.

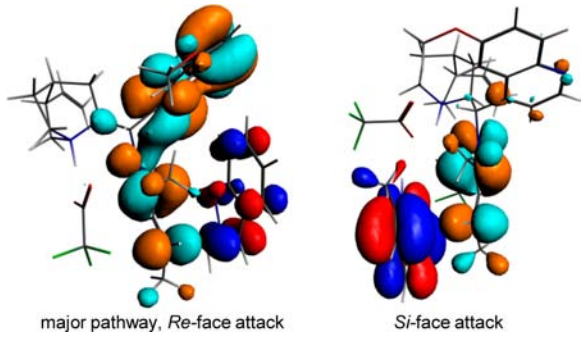

Figure 6. Frontier orbitals (HOMO red/blue and LUMO cyan/orange) of intermediate **9** for the *Re* face and *Si* face addition.

dx.doi.org/10.1021/ja404784t | J. Am. Chem. Soc. 2013, 135, 9091−9098

CONCLUSIONS

This study provides the first comprehensive picture of the mechanism of catalysis inherent to 9-amino(9-deoxy)*epi* cinchona alkaloids, a class of chiral organocatalysts widely used for the asymmetric functionalization of carbonyl compounds. A combination of experimental and theoretical investigations revealed the origin of the stereoselectivity of the Friedel–Crafts alkylation of indoles via iminium ion activation of α,β-unsaturated ketones. Our studies establish a decisive role for the acid cocatalyst, which induces the building up of a well-structured supramolecular catalytic assembly by means of electrostatic interactions. The resulting hydrogen-bonding network rigidifies the covalently bound catalyst–imine intermediate, providing the conformational constraints of the transition-state assembly required for high stereoinduction. In this system, the repulsive steric interactions between the TFA anion and the nucleophile are the defining element of stereocontrol. This is generally the case with chiral catalysts that rely on covalent interactions with substrates. Interestingly, here the cooperation of multiple attractive noncovalent interactions stabilizes the transition state leading to the major enantiomer. It is therefore also key for enantioinduction.[32]

ASSOCIATED CONTENT

Supporting Information

Complete experimental procedures, characterization data, details on kinetic studies, Cartesian coordinates and energies of all reported structures, details of computational methods, and complete ref 29c. This material is available free of charge via the Internet at http://pubs.acs.org.

AUTHOR INFORMATION

Corresponding Author

pmelchiorre@iciq.es

Notes

The authors declare no competing financial interest.

ACKNOWLEDGMENTS

Research support from the ICIQ Foundation, Spanish Ministerio de Economia y Competitividad (MINECO, grants CTQ2010-15513 and CTQ2011-29054-C02-02), the Generalitat de Catalunya (2009SGR-00259) and the European Research Council (ERC Starting Grant agreement no. 278541 - ORGA-NAUT to P.M.) is gratefully acknowledged. A.M. is grateful to MICINN for a JdC postdoctoral fellowship.

REFERENCES

(1) For reviews, see: (a) List, B. *Angew. Chem., Int. Ed.* **2010**, *49*, 1730–1734. (b) Barbas, C. F., III *Angew. Chem., Int. Ed.* **2008**, *47*, 42–47. (c) Melchiorre, P.; Marigo, M.; Carlone, A.; Bartoli, G. *Angew. Chem., Int. Ed.* **2008**, *47*, 6138–6171.

(2) (a) List, B. *Tetrahedron* **2002**, *58*, 5573–5590. (b) Jensen, K. L.; Dickmeiss, G.; Jiang, H.; Albrecht, Ł.; Jørgensen, K. A. *Acc. Chem. Res.* **2012**, *45*, 248–264. (c) Lelais, G.; MacMillan, D. W. C. *Aldrichimica Acta* **2006**, *39*, 79–87.

(3) For the seminal study on dienamine catalysis, see: Bertelsen, S.; Marigo, M.; Brandes, S.; Dinér, P.; Jørgensen, K. A. *J. Am. Chem. Soc.* **2006**, *128*, 12973–12980.

(4) For the landmark report on trienamine catalysis, see: (a) Jia, Z. J.; Jiang, H.; Gschwend, B.; Li, Q.-Z.; Yin, X.; Grouleff, J.; Chen, Y.-C.; Jørgensen, K. A. *J. Am. Chem. Soc.* **2011**, *133*, 5053–5061. For recent overviews, see: (b) Arceo, E.; Melchiorre, P. *Angew. Chem., Int. Ed.* **2012**, *51*, 5290–5292. (c) Jiang, H.; Albrecht, Ł.; Jørgensen, K. A. *Chem. Sci.* **2013**, *4*, 2287–2300.

(5) For a discussion on the mechanisms of aminocatalysis by secondary amines, see: Nielsen, M.; Worgull, D.; Zweifel, T.; Gschwend, B.; Bertelsen, S.; Jørgensen, K. A. *Chem. Commun.* **2011**, *47*, 632–649.

(6) (a) Seebach, D.; Grošelj, U.; Badine, D. M.; Schweizer, W. B.; Beck, A. K. *Helv. Chim. Acta* **2008**, *91*, 1999–2034. (b) Schmid, M. B.; Zeitler, K.; Gschwind, R. M. *Chem. Sci.* **2011**, *2*, 1793–1803. (c) Patora-Komisarska, K.; Benohoud, M.; Ishikawa, H.; Seebach, D.; Hayashi, Y. *Helv. Chim. Acta* **2011**, *94*, 719–745. (d) Burés, J.; Armstrong, A.; Blackmond, D. G. *J. Am. Chem. Soc.* **2012**, *134*, 6741–6750.

(7) (a) Cassani, C.; Martín-Rapún, R.; Arceo, E.; Bravo, F.; Melchiorre, P. *Nat. Protoc.* **2013**, *8*, 325–344. For the first synthesis of 9-amino(9-deoxy)*epi* cinchona alkaloids, see: (b) Brunner, H.; Bügler, J.; Nuber, B. *Tetrahedron: Asymmetry* **1995**, *6*, 1699–1702.

(8) (a) Melchiorre, P. *Angew. Chem., Int. Ed.* **2012**, *51*, 9748–9770. (b) Jiang, L.; Chen, Y.-C. *Catal. Sci. Technol.* **2011**, *1*, 354–365.

(9) For early studies on the activation of enones: (a) Xie, J.-W.; Chen, W.; Li, R.; Zeng, M.; Du, W.; Yue, L.; Chen, Y.-C.; Wu, Y.; Zhu, J.; Deng, J.-G. *Angew. Chem., Int. Ed.* **2007**, *46*, 389–392. Ketones: (b) Liu, T.-Y.; Cui, H.-L.; Zhang, Y.; Jiang, K.; Du, W.; He, Z.-Q.; Chen, Y.-C. *Org. Lett.* **2007**, *9*, 3671–3674. α-Branched aldehydes: (c) McCooey, S. H.; Connon, S. J. *Org. Lett.* **2007**, *9*, 599–602. α-Branched enals: (d) Galzerano, P.; Pesciaioli, F.; Mazzanti, A.; Bartoli, G.; Melchiorre, P. *Angew. Chem., Int. Ed.* **2009**, *48*, 7892–7894. α-Branched enones: (e) Tian, X.; Cassani, C.; Liu, Y.; Moran, A.; Urakawa, A.; Galzerano, P.; Arceo, E.; Melchiorre, P. *J. Am. Chem. Soc.* **2011**, *133*, 17934–17941.

(10) For dienamine activation: (a) Bencivenni, G.; Galzerano, P.; Mazzanti, A.; Bartoli, G.; Melchiorre, P. *Proc. Natl. Acad. Sci. U.S.A.* **2010**, *107*, 20642–20647. (b) Bergonzini, G.; Vera, S.; Melchiorre, P. *Angew. Chem., Int. Ed.* **2010**, *49*, 9685–9688. For trienamine activation: (c) Xiong, X.-F.; Zhou, Q.; Gu, J.; Dong, L.; Liu, T.-Y.; Chen, Y.-C. *Angew. Chem., Int. Ed.* **2012**, *51*, 4401–4404. For vinylogous iminium ion activation, see: (d) Tian, X.; Liu, Y.; Melchiorre, P. *Angew. Chem., Int. Ed.* **2012**, *51*, 6439–6442. (e) Tian, X.; Melchiorre, P. *Angew. Chem., Int. Ed.* **2013**, *52*, 5360–5363.

(11) For sporadic mechanistic studies on cinchona-based primary aminocatalysis, see: (a) Su, Z.; Lee, H. W.; Kim, C. K. *Eur. J. Org. Chem.* **2013**, 1706–1715. (b) Lifchits, O.; Mahlau, M.; Reisinger, C. M.; Lee, A.; Farès, F.; Polyak, I.; Gopakumar, G.; Thiel, W.; List, B. *J. Am. Chem. Soc.* **2013**, *135*, 6677–6693. For recent studies on asymmetric transformations promoted by cinchona alkaloid-based catalysts, see: (c) Li, H.; Liu, X.; Wu, F.; Tang, L.; Deng, L. *Proc. Natl. Acad. Sci. U.S.A.* **2010**, *107*, 20625–20629. (d) Su, Z.; Lee, H. W.; Kim, C. K. *Org. Biomol. Chem.* **2011**, *9*, 6402–6409. (e) Zhu, J.-L.; Zhang, Y.; Liu, C.; Zheng, A.-M.; Wang, W. *J. Org. Chem.* **2012**, *77*, 9813–9825.

(12) For examples demonstrating the potential of combining theoretical and experimental studies to elucidate the mechanism of organocatalytic transformations, see: (a) Lin, S.; Jacobsen, E. N. *Nat. Chem.* **2012**, *4*, 817–824. (b) Xu, H.; Zuend, S. J.; Woll, M. G.; Tao, Y.; Jacobsen, E. N. *Science* **2010**, *327*, 986–989. (c) Bahmanyar, S.; Houk, K. N.; Martin, H. J.; List, B. *J. Am. Chem. Soc.* **2003**, *125*, 2475–2479.

(13) For a comprehensive review on quantum mechanical investigations of organocatalysis, see: (a) Cheong, P. H.-Y.; Legault, C. Y.; Um, J. M.; Celebi-Ölçüm, N.; Houk, K. N. *Chem. Rev.* **2011**, *111*, 5042–5137. For selected examples, see: (b) Um, J. M.; Gutierrez, O.; Schoenebeck, F.; Houk, K. N.; MacMillan, D. W. C. *J. Am. Chem. Soc.* **2010**, *132*, 6001–6005. (c) Pierce, M. D.; Johnston, R. C.; Mahapatra, S.; Yang, H.; Carter, R. G.; Cheong, P. H.-Y. *J. Am. Chem. Soc.* **2012**, *134*, 13624–13631. (d) Dieckmann, A.; Breugst, M.; Houk, K. N. *J. Am. Chem. Soc.* **2013**, *135*, 3237–3242.

(14) Chen, W.; Du, W.; Yue, L.; Li, R.; Wu, Y.; Ding, L.-S.; Chen, Y.-C. *Org. Biomol. Chem.* **2007**, *5*, 816–821.

(15) Bartoli, G.; Carlone, A.; Pesciaioli, F.; Sambri, L.; Melchiorre, P. *Org. Lett.* **2007**, *9*, 1403−1405.
(16) As detailed in the original report (ref 15), when using the racemic or the opposite (L)-enantiomer of the *N*-Boc phenylglycine in combination with **1b**, the same sense of asymmetric induction with very similar selectivity, although with slightly different reactivity, was observed in the Friedel−Crafts reaction. The absence of a marked matched/mismatched catalyst ion pair combination suggests the pK_a of the acid, and not its three-dimensional structure, as the factor influencing the catalysis.
(17) For a review on supramolecular catalytic species, assembled by harnessing multiple weak intramolecular interactions, see: Meeuwissen, J.; Reek, J. N. H. *Nat. Chem.* **2010**, *2*, 615−621.
(18) For a review, see: (a) Mahlau, M.; List, B. *Angew. Chem., Int. Ed.* **2013**, *52*, 518−533. For the seminal report, see: (b) Mayer, S.; List, B. *Angew. Chem., Int. Ed.* **2006**, *45*, 4193−4195.
(19) The iminium ion formation is accelerated under acidic conditions, see: (a) Evans, G. J. S.; White, K.; Platts, J. A.; Tomkinson, N. C. O. *Org. Biomol. Chem.* **2006**, *4*, 2616−2627. (b) Jenks, W. P. *Catalysis in Chemistry and Enzymology*; McGraw-Hill: New York, 1969; Chapter 10, Section B, Part 1.
(20) (a) Lu, X.; Deng, L. *Angew. Chem., Int. Ed.* **2008**, *47*, 7710−7713. (b) Singh, R. P.; Bartelson, K.; Wang, Y.; Su, H.; Lu, X.; Deng, L. *J. Am. Chem. Soc.* **2008**, *130*, 2422−2423. (c) Wang, X.; Reisinger, C. M.; List, B. *J. Am. Chem. Soc.* **2008**, *130*, 6070−6071. (d) Lu, X.; Liu, Y.; Sun, B.; Cindric, B.; Deng, L. *J. Am. Chem. Soc.* **2008**, *130*, 8134−8135.
(21) Extensive studies aimed at identifying the best ratio between [HMPA] and [TFA] are detailed in Figure S6 within the SI. The ability of HMPA to suppress the acid-catalyzed pathway led to a consistent profile of the enantioselectivity (ee in the range of 83−85% ee, Figure 2).
(22) Strong Brønsted acids can catalyze the Friedel-Craft reaction of indoles with enones, see for examples: (a) Zhou, W.; Xu, L.-W.; Li, L.; Yang, L.; Xia, C.-G. *Eur. J. Org. Chem.* **2006**, 5225−5227. (b) Tang, H.-Y.; Lu, A.-D.; Zhou, Z.-H.; Zhao, G.-F.; He, L.-N.; Tang, C.-C. *Eur. J. Org. Chem.* **2008**, 1406−1410.
(23) The presence of an acid-promoted racemic pathway that competes with the stereoselective aminocatalytic regime would preclude the possibility of a mechanistic study, since both the rate and the ee of the reaction are altered. The presence of HMPA, due to its hydrogen-bond-accepting ability, greatly reduces the rate of the acid-catalyzed process by sequestering the free TFA that is not engaged in electrostatic interactions with the basic moieties of catalyst **1a**. Extensive studies, detailed in Section B and Scheme S1 within the SI, indicate that the role of HMPA is to suppress the acid-catalyzed pathway, thus providing a reliable catalytic system for our mechanistic studies. HMPA has a minimal influence, if any, on the organocatalytic regime.
(24) This approach relies on graphical manipulation of the extensive data sets available from accurate in situ monitoring of reaction progress under conditions where two concentration variables are changing simultaneously. (a) Blackmond, D. G. *Angew. Chem., Int. Ed.* **2005**, *44*, 4302−4320. (b) Mathew, J. S.; Klussmann, M.; Iwamura, H.; Valera, F.; Futran, A.; Emanuelsson, E. A. C.; Blackmond, D. G. *J. Org. Chem.* **2006**, *71*, 4711−4722. (c) Helfferich, F. G. *Kinetics of Homogeneous Multi-Step Reactions*; Elsevier: Amsterdam, 2001; Chapter 7.2.
(25) Repeating the RPKA of the model reaction catalyzed by the **1a**·$(TFA)_2$ combination (2 equiv of TFA) gave a very similar kinetic profile; see Section D3 within the SI for full details. This is why the **1a**·$(TFA)_2$ catalyst system was used within the computational investigations.
(26) This technique has demonstrated its efficiency for mechanistic studies, see for examples: (a) Zotova, N.; Franzke, A.; Armstrong, A.; Blackmond, D. G. *J. Am. Chem. Soc.* **2007**, *129*, 15100−15101. (b) Zotova, N.; Broadbelt, L. J.; Armstrong, A.; Blackmond, D. G. *Bioorg. Med. Chem. Lett.* **2009**, *19*, 3934−3937. (c) Shekhar, S.; Ryberg, P.; Hartwig, J. F.; Mathew, J. S.; Blackmond, D. G.; Strieter, E. R.; Buchwald, S. L. *J. Am. Chem. Soc.* **2006**, *129*, 3584−3591. (d) Nielsen, L. P. C.; Stevenson, C. P.; Blackmond, D. G.; Jacobsen, E. N. *J. Am. Chem. Soc.* **2004**, *127*, 1360−1362.
(27) The parameters of the "power-law" given in eq 1 were determined by nonlinear least-squares fitting of the data to the rate law between 10−90% conversion by using the Solver function within Microsoft Excel. The confidence intervals have been established according to the procedure described in: Kemmer, G.; Keller, S. *Nat. Protoc.* **2010**, *5*, 267−281.
(28) Precedent kinetic studies on iminium ion-catalyzed reactions using chiral secondary amines have identified the C−C bond formation as the rate-limiting step, see: (a) Evans, G.; Gibbs, T. J. K.; Jenkins, R. L.; Coles, S. J.; Hirsthouse, M. B.; Platts, J. A.; Tomkinson, N. C. O. *Angew. Chem., Int. Ed.* **2008**, *47*, 2820−2823. (b) Lakhdar, S.; Tokuyasu, T.; Mayr, H. *Angew. Chem., Int. Ed.* **2008**, *47*, 8723−8727.
(29) (a) Zhao, Y.; Truhlar, D. G. *Theor. Chem. Acc.* **2008**, *120*, 215−241. (b) Marenich, A. V.; Cramer, C. J.; Truhlar, D. G. *J. Phys. Chem. B* **2009**, *113*, 6378−6396. (c) Frisch, M. J.; et al. *Gaussian 09*, revision A.02; Gaussian, Inc.: Wallingford CT, 2009.
(30) Using DFT-based methods, we optimized the relative energies of different possible geometries for the iminium ion species **A**. Details are available in Section E3 of the SI. We also performed nuclear magnetic resonance (NMR) spectroscopic investigations to characterize the iminium ion assembly **A**. While the imine precursor was fully chracterized, our extensive attempts to form an iminium ion in situ in the presence of different acids were met with failure, due to the unstable nature of the ion pair intermediate.
(31) For a DFT study of a similar Friedel−Crafts process with enals catalyzed by a secondary amine, see: Gordillo, R.; Carter, J.; Houk, K. N. *Adv. Synth. Catal.* **2004**, *346*, 1175−1185.
(32) Knowles, R. R.; Jacobsen, E. N. *Proc. Natl. Acad. Sci. U.S.A.* **2010**, *107*, 20678−20685.